

Why does adding a poor thermal conductor increase propagation rate in solid propellants?

Cite as: Appl. Phys. Lett. **115**, 114101 (2019); <https://doi.org/10.1063/1.5113612>

Submitted: 05 June 2019 . Accepted: 14 August 2019 . Published Online: 09 September 2019

 Dylan J. Kline,  Miles C. Rehwoldt,  Haiyang Wang,  Noah E. Eckman, and  Michael R. Zachariah



View Online



Export Citation



CrossMark

ARTICLES YOU MAY BE INTERESTED IN

[Drainage of lubrication film around stuck bubbles in vertical capillaries](#)

Applied Physics Letters **115**, 111601 (2019); <https://doi.org/10.1063/1.5112055>

[Two-terminal terahertz detectors based on AlGaIn/GaN high-electron-mobility transistors](#)

Applied Physics Letters **115**, 111101 (2019); <https://doi.org/10.1063/1.5114682>

[Achieving self-guiding unidirectional electromagnetic bulk states by breaking time-mirror symmetry](#)

Applied Physics Letters **115**, 111902 (2019); <https://doi.org/10.1063/1.5111053>



Your Qubits. Measured.

Meet the next generation of quantum analyzers

- Readout for up to 64 qubits
- Operation at up to 8.5 GHz, mixer-calibration-free
- Signal optimization with minimal latency

Find out more



Why does adding a poor thermal conductor increase propagation rate in solid propellants?

Cite as: Appl. Phys. Lett. **115**, 114101 (2019); doi: [10.1063/1.5113612](https://doi.org/10.1063/1.5113612)

Submitted: 5 June 2019 · Accepted: 14 August 2019 ·

Published Online: 9 September 2019



View Online



Export Citation



CrossMark

Dylan J. Kline,^{1,2}  Miles C. Rehwoldt,^{1,2}  Haiyang Wang,²  Noah E. Eckman,¹  and Michael R. Zachariah^{2,a)} 

AFFILIATIONS

¹Department of Chemical and Biomolecular Engineering, University of Maryland College Park, College Park, Maryland 20742, USA

²Department of Chemical and Environmental Engineering, University of California Riverside, Riverside, California 92521, USA

^{a)}Author to whom correspondence should be addressed: mrz@engr.ucr.edu

ABSTRACT

Solid propellant additives have a long history of modulating burning rate by introducing materials with high thermal diffusivities to better concentrate and transfer heat to nearby areas. However, recent studies have demonstrated a counterintuitive result in that additives with thermally insulating properties—notably SiO₂ particles—can also enhance the propagation rate in solid propellants. In this work, high-speed microscopy and thermometry were performed on 3D printed solid propellant films containing both thermally conducting (graphite) and insulating (SiO₂) particles to investigate the role of these additives on film propagation rate. It was found that addition of SiO₂ particles increased the effective surface area of the reaction front through inhomogeneous heat transfer in the films, and that such corrugation of the reaction front area on the micrometer scale manifests itself as a global increase in the propagation rate on the macro scale. Graphite additive was observed to have a substantially lower burning surface area and propagation rate, suggesting that the effect of reaction front surface area is larger than the effect of thermal diffusivity for low-weight percent additives in solid propellants.

Published under license by AIP Publishing. <https://doi.org/10.1063/1.5113612>

Energetic materials—the overarching class of pyrotechnics, propellants, and explosives—have received a renewed interest in the scientific community with investigations into new formulations,^{1–6} physical architectures,^{7–9} and expanding applications to the civilian and military communities. Considering new advances in nanomaterial production and additive manufacturing, solid rocket propellants have experienced a particular rise in research aimed at determining the underlying thermochemical mechanisms that govern their combustion performance and capitalize on their customizability and ease of production.^{8–11} Among the most important parameters of solid propellants driven by in the chemical formulation are the combustion temperature and the propellant burn rate.¹² Temperature of combustion dictates the theoretical maximum force that can be achieved in the expanding gases given a constrained velocity while propagation rate determines the time over which this force can be applied. Considering that only certain materials are traditionally employed as fuels (Al) and binders (HTPB) in solid propellants, modifying the propagation rate is a primary route by which to modulate the combustion performance. In the gas phase, the steady-state propagation velocity (v) theoretically scales with the thermal diffusivity (α) of the combusting material and the chemical reaction rate ($\dot{\omega}$) as shown in Eq. (1),

$$v \propto \sqrt{\alpha \cdot \dot{\omega}}. \quad (1)$$

One can reasonably conjecture that similar controlling processes might occur in the condensed phase. Modulation of combustion performance for solid propellants has a long history of capitalizing on embedding materials with a high thermal diffusivity. Space-race age reports by Caveny and Glick¹³ demonstrate the principles upon which the addition of a wire with a high thermal diffusivity can dramatically increase the propagation rate in a solid propellant by enhancing heat conduction to different areas of the propellant. These “wired propellants” have since been widely used and the dominating characteristics of their combustion performance is a distinct cone shape in the burning surface structure that is thought to increase the burning surface area, and thus the propagation rate.^{14–16} More recent experiments by Isert *et al.* capture the same cone structure and enhanced burning rate.¹⁶

Recent results by our group¹⁷ and others,¹⁸ however, demonstrate a uniquely different phenomena with the addition of thermally insulating particles that are embedded during material synthesis. Wang *et al.*¹⁷ incorporated mesoporous silicon dioxide—a material commonly used for thermal insulation—into reactive nanoaluminum polyvinylidene fluoride (Al/PVDF) films prepared by electrospinning and noticed a $\sim 3x$ increase in burn rate at 2.5 weight percent SiO₂. To

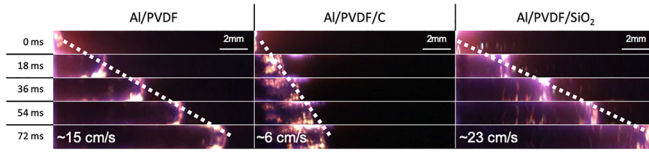


FIG. 1. Macroscale burn rate images of a printed film on a microscope slide at 5000 frames/s. Burn time measured from ignition to the time that the reaction front reaches the end of the microscope slide. Note: propagation is from left-to-right.

explain this, the authors suggested that the particles generated hot spots and effectively increased the number of ignition sites in the material, however direct evidence was not presented in the study.¹⁷ Wang *et al.* also show evidence of meso-SiO₂ interaction with the fluorine compounds in the reactive system with TGA/DSC and MS; however, experiments with micrometer-SiO₂ at the same mass loading had a reduced overall decomposition, likely attributable to the lower surface area of the micro-SiO₂.¹⁷ Thermogravimetric analysis by Shioya *et al.* showed no catalytic interaction of SiO₂ in their Al/AP/HTPB system, but also reported an increased overall burn rate with the addition of low weight percent SiO₂.¹⁸

To determine why previous research has demonstrated an enhanced propagation rate in 3D printed solid propellants when doped with poor thermal conductors, two scenarios were evaluated: (i) addition of poor thermal conducting particles (SiO₂) and (ii) addition of a good thermal conductor (Graphite/Carbon). Films were prepared by dissolving 300 mg polyvinylidene fluoride (PVDF, average molecular weight ~534 000) in 5 ml of dimethylformamide (DMF, 99.8%) and subsequently adding 300 mg aluminum nanoparticles (Novacentrix, ~85 nm, ~81% active weight) for an equivalence ratio (Φ) of 2.87. The mixtures were then each sonicated for a half hour, after which 15.4 mg of silicon dioxide micrometer particles (SiO₂ 1–5 μ m, Sigma Aldrich) and 15.4 mg of graphite flakes (Alfa Aesar) were added to the two mixtures, respectively, for an average loading of 2.5% by weight. The two mixtures were then sonicated for another half hour and magnetically

stirred for 24 h. As prepared inks were then printed with a Hyrel 30M 3D onto microscope coverslips (VWR 0.17 mm thickness, 22 mm²) over an 80 °C preheated plate in an 8 cm² pattern at a flow rate of ~0.3 ml/min and speed of ~22 cm/min.

Scanning electron microscopy images of the doped Al/PVDF samples are presented in Fig. S1. The Al/PVDF/C film on the left shows a relatively even distribution of the micrometer-sized graphite particles embedded into the printed film's cross section. The Al/PVDF/SiO₂ film cross section shows large agglomerations of particles and a much more cavernous cross section with SiO₂ particles (1–5 μ m) distributed within the frame. It is important to note that porosity of the films does alter the propagation rate in the materials, however this impact would likely be less evident for material that was firmly adhered to the microscope slides.^{9,10}

Combustion of the samples was then visualized using a Vision Research Phantom VEO710L camera at 5000 frames/s at both the macro- and microscale. In both sets of tests, samples printed on the coverslips were mounted vertically on a 3-axis translational stage (Newport), brought into focus, and ignited using a resistively heated nichrome wire. For the macro tests shown in Fig. 1, the burn time was the time it took from ignition of the material to the completed propagation across the 22 mm slide. Quite clearly, we see that, when compared to the nascent Al/PVDF base case, addition of carbon (a good thermal conductor) slows the reaction front, while addition of silica (a poor thermal conductor) speeds up the reaction front. This is in direct contradiction to that predicted by Eq. (1). We now turn to the microscopic imaging.

Evaluation of the combustion characteristics at the microscale used a house-built high-speed microscope assembly in which the ignition event is observed using light passed through a 40 \times microscope objective (Nikon) which is transmitted through a beam splitter, through a camera lens (Nikon 105 mm Macro) focused at infinity, and onto the camera sensor.¹⁹ With the microscope objective, the pixel resolution of the camera assembly is ~1 μ m/pixel and allows us to resolve an approximate the reaction front length and initial topography of the film (see Fig. S1).

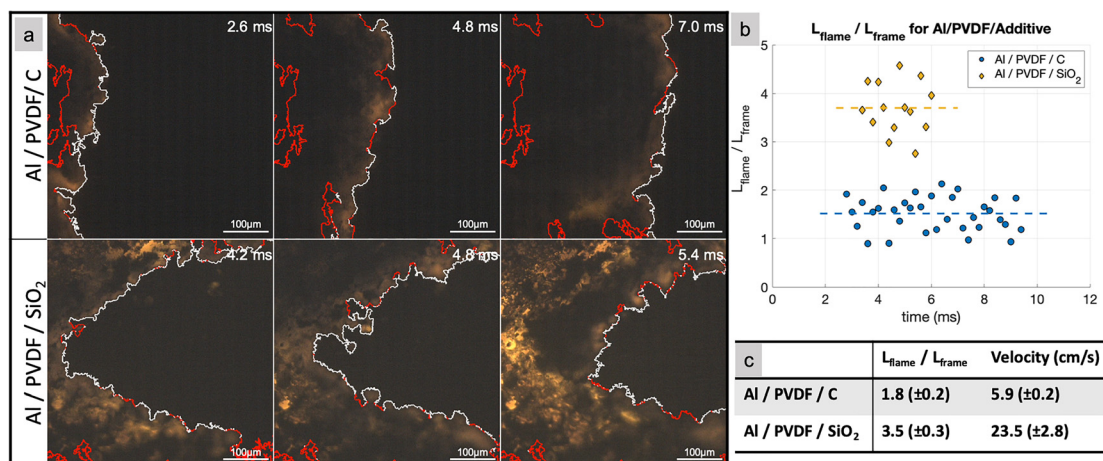


FIG. 2. High-speed microscopy images for (a) Al/PVDF/C and (b) Al/PVDF/SiO₂ with outlines of reaction front. Red lines represent regions that had not moved within 2 frames. (c) Plots of window-size normalized flame length as a function of time for Al/PVDF/C and Al/PVDF/SiO₂. (d) Average flame length and velocity for additive-doped films. Note: propagation is from left-to-right.

Microscale videos were post processed to determine an estimated reaction front length and velocity distribution. Images are imported using a custom MATLAB routine which provides raw pixel intensities for each image and the images are subsequently binarized using MATLAB's Image Processing Toolbox.²⁰ The length of the reaction front only considers those points that had moved within the previous two frames of the recorded video as identified by the binarization routine.

Figure 2 demonstrates the effect of C and SiO₂ additives on the effective reaction front length of the propagating Al/PVDF films. Very similar behavior was also observed by Merzhanov *et al.*, in their studies of gasless combustion of Ti with Si.²¹ The Al/PVDF/C additive has a relatively linear reaction front that has larger corrugated areas spanning the entire length of the window [Fig. 2(a)]. However, the Al/PVDF/SiO₂ front has many more small corrugations spread out over the entire length which effectively increases the surface area of the burning front [Fig. 2(b)]. Using these results, we can plot a normalized reaction front length ($L_{\text{flame}}/L_{\text{frame}}$) in Fig. 3(c), which clearly quantifies that both composites have a steady reaction front length for the few milliseconds that the film is within view, and that the length of the Al/PVDF/SiO₂ front is $\sim 2\times$ longer than that in the Al/PVDF/C case. When averaging the reaction front length over three separate tests, this twofold increase in reaction front length remains consistent [Fig. 2(d)]. Also from Fig. 2(d), the global-average velocity of the macro-scale burn tests appears to increase in accordance with reaction front length—a reasonable expectation since burn rate in solid propellants is directly related to the burning surface area.¹²

To further investigate these observations, we consider how the local velocity might be changing and how it impacts the global average velocity observed. Local velocities of the points along the reaction front were determined by using a closest-point determination between the active reaction front in one frame to the next frame and dividing by

the framerate (5000 fps). Sample images of the Al/PVDF composite films along with their reaction front areas and estimated velocity vectors are shown in Figs. 3(a)–3(c), where we continue to see a relatively constant velocity vector length along the Al/PVDF/C front and a wider distribution over the length of the Al/PVDF/SiO₂ front. Histograms of the Al/PVDF/C and Al/PVDF/SiO₂ calculated velocity vectors summed over the length of each video are presented in Figs. 3(b)–3(d) and, while the distribution of velocities is wider in the Al/PVDF/SiO₂ case, the average local velocities are both ~ 5.5 cm/s. Considering local velocities are similar for both cases tested, the observed effect on global burn rate can be attributed to the corrugation in the reaction front rather than any specific enhanced chemistry that drives reactions faster.

Temperature maps of the high-speed microscopy images were used to evaluate the plausibility of inhomogeneous heat transfer on the reaction front for both additives. Briefly, temperature measurements can be extracted using the color video camera using channel intensity ratios for the different colors of the filter array placed in front of the camera sensor, assuming graybody behavior of the burning material, and integrating the expected light intensity for each color channel for the entire light spectrum over which the camera is sensitive. More details on the methodology can be found in our prior work.² Careful observation of the reaction fronts in the original color images show that, for the Al/PVDF/SiO₂ samples, we can see the emergence of distinct bright regions which lead to lagging edges in the following frames (see Fig. 4). Pyrometry measurements made on these images show the evolution of hot spots with localized temperatures 300–400 K higher than the rest of the reaction front where the silica particles were observed in the before image. It is therefore believed that the lagging edge in the reaction front was induced by the additive particles which thereby increased the surface area of the burning front.

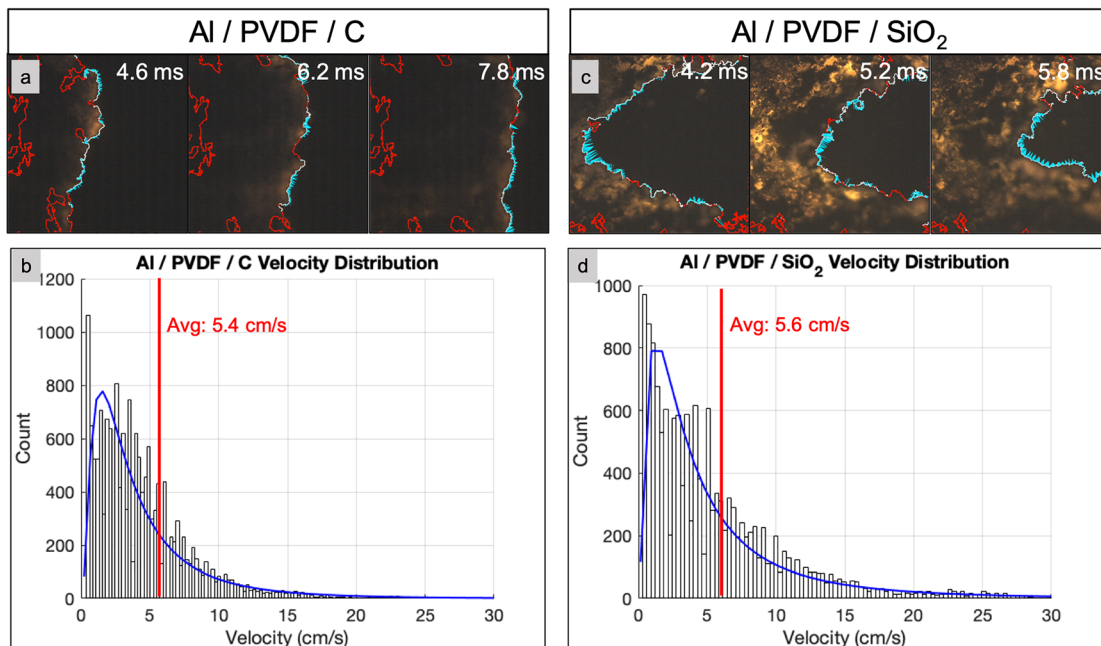


FIG. 3. (a) Al/PVDF/C and (c) Al/PVDF/SiO₂ imaged through high-speed microscopy with area outline (red/white) and velocity vectors (blue). Histogram of measured velocities for (b) Al/PVDF/C and (d) Al/PVDF/SiO₂.

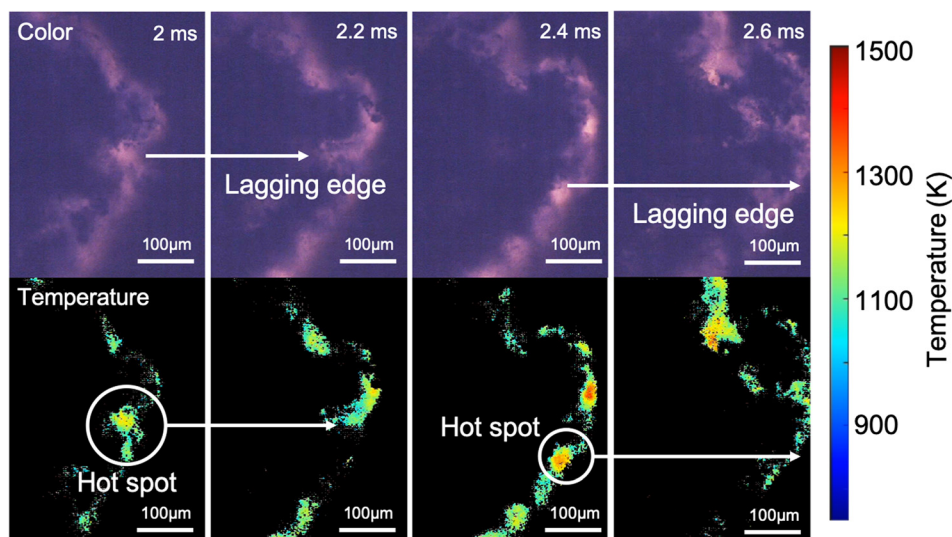


FIG. 4. (Top) high-speed microscopy images and (bottom) corresponding temperature maps obtained by color camera pyrometry.

As previously discussed, the burn rate of a solid propellant is estimated to scale directly with the burning surface area (A), however it is also proposed to scale with the square root of thermal diffusivity (α) and the chemical reaction rate ($\dot{\omega}$). When only considering the effect of thermal diffusivity on the propagation velocity, it would be expected that the carbon additive ($\alpha \sim 200 \text{ mm}^2/\text{s}$)²² would burn much faster than the SiO_2 -doped composite ($\alpha \sim 0.8 \text{ mm}^2/\text{s}$)²³ because of faster heat feedback in the latter, but the exact opposite behavior was observed. Mass-average estimations of thermal diffusivity presented in Table S1 show that, on a bulk scale, the low weight percent additives change α of the Al/PVDF $\Phi = 2.87$ ($\alpha \sim 48 \text{ mm}^2/\text{s}$) less than 10%, suggesting that the observed burn rate modulation is dominated on the microscale where differences in local α change by orders of magnitude.²⁴ Thus, the observed change in burn rate is likely because, at low mass loadings, the SiO_2 additive is stochastically modulating the heat transfer, resulting in an inhomogeneous thermal profile. This in turn leads to corrugation of the reaction front, thus increasing burning surface area and the mass burning rate which, at the macroscale, is observed as an increase in the global reaction front velocity. Carbon, in contrast with its higher thermal conductivity, more evenly distributes the released energy along the burning surface so that all regions have effectively the same local velocity, resulting in a flatter reaction front with lower surface area. This mechanism of enhanced propagation velocity likely breaks down, however, at higher mass loadings or in scenarios where a concentrated region of high thermal diffusivity enhances heat transfer on a bulk scale and creates a burning rate gradient that also effectively increases the burning surface area.

The counterintuitive observation that thermally insulating additives increase burn rate in solid propellants can therefore be attributed to the role that burning surface area plays on the propagation rate. High-speed microscopy suggests that inhomogeneous heat transfer in the burning films leads to increased corrugation of the reaction front when the additives are homogeneously dispersed in the film at low mass-percentages. This observation therefore suggests that, as an alternative to large conductive wires being added to propellants in the manufacturing stage of rocket motors, engineers could instead

introduce small masses of thermally insulating particles to increase the effective burning surface area and burning rate.

See the [supplementary material](#) for scanning electron microscopy images of the as-prepared Al/PVDF/additive films and their respective elemental maps are included in the supplementary file. Images of the Al/PVDF/additive films as observed with the high-speed microscope prior to combustion are also included. Thermal diffusivity values of the materials used are tabulated and used to estimate bulk thermal diffusivity of the test materials.

The authors gratefully acknowledge support from the Army Research Office and the Air Force Office of Scientific Research.

REFERENCES

- ¹V. E. Zarko and A. A. Gromov, *Energetic Nanomaterials: Synthesis, Characterization, and Application* (Elsevier, 2016).
- ²R. J. Jacob, D. J. Kline, and M. R. Zachariah, *J. Appl. Phys.* **123**, 115902 (2018).
- ³D. K. Smith, D. K. Unruh, C.-C. Wu, and M. L. Pantoya, *J. Phys. Chem. C* **121**, 23192 (2017).
- ⁴T. Wu, X. Wang, P. Y. Zavalij, J. B. DeLisio, H. Wang, and M. R. Zachariah, *Combust. Flame* **191**, 335 (2018).
- ⁵P. M. Guerieri, S. DeCarlo, B. Eichhorn, T. Connell, R. A. Yetter, X. Tang, Z. Hicks, K. H. Bowen, and M. R. Zachariah, *J. Phys. Chem. A* **119**, 11084 (2015).
- ⁶M. C. Rehwoldt, Y. Yang, H. Wang, S. Holdren, and M. R. Zachariah, *J. Phys. Chem. C* **122**, 10792 (2018).
- ⁷C. Rossi, *Propellants, Explos., Pyrotech.* **44**, 94 (2018).
- ⁸I. E. Gunduz, M. S. McClain, P. Cattani, G. T. C. Chiu, J. F. Rhoads, and S. F. Son, *Addit. Manuf.* **22**, 98 (2018).
- ⁹H. Wang, D. Kline, M. Rehwoldt, T. Wu, W. Zhao, X. Wang, and M. R. Zachariah, *ACS Appl. Polym. Mater.* **1**, 982 (2019).
- ¹⁰K. T. Sullivan, C. Zhu, E. B. Duoss, A. E. Gash, D. B. Kolesky, J. D. Kuntz, J. A. Lewis, and C. M. Spadaccini, *Adv. Mater.* **28**, 1934 (2016).
- ¹¹A. S. Mukasyan, A. S. Rogachev, M. Mercedes, and A. Varma, *Chem. Eng. Sci.* **59**, 5099 (2004).
- ¹²G. P. Sutton and O. Biblarz, *Rocket Propulsion Elements*, 8th ed. (Wiley, 2011).
- ¹³L. H. Caveny and R. L. Glick, *J. Spacecr. Rockets* **4**, 79 (1967).
- ¹⁴N. Kubota, M. Ichidat, and T. Fujisawa, *AIAA J.* **20**, 116 (1982).

- ¹⁵C. Shuling and L. Fengsheng, *Combust. Flame* **45**, 213 (1982).
- ¹⁶S. Isert, C. D. Lane, I. E. Gunduz, and S. F. Son, *Proc. Combust. Inst.* **36**, 2283 (2017).
- ¹⁷H. Wang, J. B. DeLisio, S. Holdren, T. Wu, Y. Yang, J. Hu, and M. R. Zachariah, *Adv. Eng. Mater.* **20**, 1700547 (2018).
- ¹⁸S. Shioya, M. Kohga, and T. Naya, *Combust. Flame* **161**, 620 (2014).
- ¹⁹H. Wang, D. J. Kline, and M. R. Zachariah, *Nat. Commun.* **10**, 3032 (2019).
- ²⁰MathWorks Image Processing Toolbox software (2019), <https://www.mathworks.com/help/images/>.
- ²¹A. G. Merzhanov, A. S. Mukasyan, A. S. Rogachev, A. E. Sychev, S. Wang, and A. Varma, *Combust. Explos. Shock Waves* **32**, 655 (1997).
- ²²H. Nagano, H. Kato, A. Ohnishi, and Y. Nagasaka, *High Temp. - High Press.* **33**, 253 (2001).
- ²³T. Katsura, *Phys. Chem. Miner.* **20**, 201 (1993).
- ²⁴J. Yu, R. Qian, and P. Jiang, *Fibers Polym.* **14**, 1317 (2013).